Materials Advances

ROYAL SOCIETY OF CHEMISTRY

PAPER

View Article Online
View Journal

Cite this: DOI: 10.1039/d6ma00475j

Photophysical properties of a highly delocalized allylic cation: acid-independent and solvent-dependent intramolecular charge transfer

Jiaoyan Zhao,†[ab] Bradley A. Tavana,†[c] Seongje Park,†[cd] Max Jacobsen,[ab] Nicholas Woodlief,[ab] Erin Locke,[ab] Rebecca M. Gracia,[cd] Cedric Schaack*[ab] and Minjung Son*[cd]

Received 6th April 2026,
Accepted 1st June 2026

DOI: 10.1039/d6ma00475j

rsc.li/materials-advances

Tetraarylallenes that form highly delocalized allylic cations upon activation represent an emerging class of charge-transfer chromophores. Here, we investigate the solvent- and cation-dependent photophysical properties of a donor–acceptor substituted allene that generates an extended polymethine-like cation upon protonation or Lewis acid coordination. Steady-state spectroscopy reveals pronounced solvatochromism of the activated species, and femtosecond transient absorption measurements further demonstrate that the excited-state lifetimes are strongly dependent on solvent polarity. In contrast, variation of the activating acid does not impact the spectral features and excited-state dynamics, indicating that the photophysical response is governed by the intrinsic electronic structure of the delocalized allylic cation rather than specific counterion effects. These results provide fundamental insight into the environmental modulation of charge-transfer character and establish guiding principles for the design of robust, stimuli-responsive optical materials.

Introduction

Stimuli-responsive materials are a class of "smart" systems that dynamically adapt their properties in response to environmental cues such as heat,[1–3] light,[4,5] or pH,[6] opening the door to emerging technologies including self-healing polymers, shape-morphing robotics, and precisely targeted medical treatments.[7–16] At the heart of many of these advanced materials are charge-transfer (CT) chromophores, whose electronic structures are exquisitely sensitive to their local environment, allowing them to function as molecular triggers for macroscopic responses.[17–21] Elucidating how local environments govern the electronic structure and photophysical behavior of these compounds remains a central challenge in physical organic chemistry.

One of the most direct and powerful approaches to probing these environment-dependent effects is through solvatochromism. Solvatochromic shifts in absorption and emission spectra provide detailed insight into the nature of electronic transitions, the extent of charge redistribution in excited states, and the interplay between molecular structure and its surrounding environment.[22–27] These structure–property relationships are particularly pronounced in systems that exhibit intramolecular charge transfer (ICT) character, where electronic excitation induces substantial charge reorganization across the molecular framework.[28,29] Merocyanine and nitroaromatic dyes have long dominated the landscape of solvatochromic reporters[30–37]; however, the growing demand for advanced responsive materials is now driving efforts to expand the chromophore library to include nontraditional π systems with enhanced structural rigidity and electronic tunability.

Allenes, characterized by two consecutive double bonds (C═C═C), represent an intriguing scaffold for the development of modern solvatochromic probes.[38,39] Unlike planar polyenes, the orthogonal arrangement of the π systems in allenes enables distinct electronic transitions and chiroptical responses that can be highly sensitive to the local environment.[40] Recently, we reported that tetraaryl-substituted allenes undergo reversible protonation at the central sp-hybridized carbon, triggering dramatic bathochromic shifts of up to 500 nm and generating allylic cations with extended π-conjugation and polymethine-like electronic character (Fig. 1a and b).[11] Notably, the protonated species exhibit remarkable spectral tunability spanning the visible to near-infrared regions. The ability to reversibly toggle between the neutral allene and the highly conjugated allylic cation, accompanied by a pronounced, stimuli-responsive "turn-on"

[a] Department of Chemistry, Wake Forest University, 1834 Wake Forest Road, Winston-Salem, NC 27109, USA. E-mail: schaacc@wfu.edu
[b] Center for Functional Materials, Wake Forest University, 1834 Wake Forest Road, Winston-Salem, NC 27109, USA
[c] Department of Chemistry, Boston University, 590 Commonwealth Avenue, Boston, MA 02215, USA. E-mail: mson@bu.edu
[d] Boston University Photonics Center, 8 Saint Mary's Street, Boston, MA 02215, USA
† These authors contributed equally to this work.

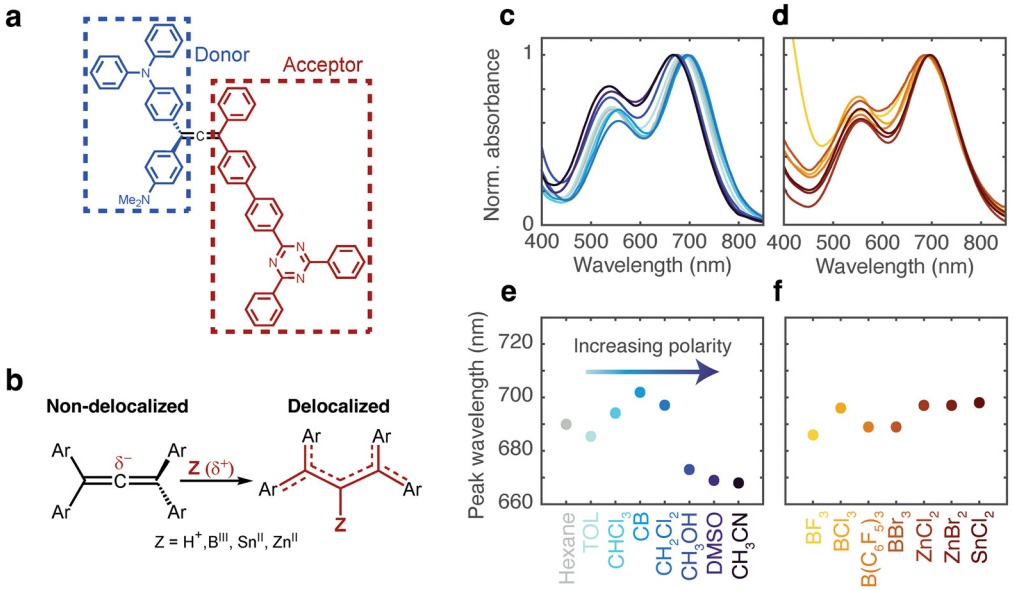

Fig. 1 (a) Chemical structure of the allene investigated in this work. (b) Schematic representation illustrating the conversion of the allene to a delocalized allylic species upon addition of a Brønsted or Lewis acid. (c) and (d) Normalized steady-state absorption spectra of the protonated allene measured in (c) a series of organic solvents with increasing polarity (hexane, toluene (TOL), chloroform, chlorobenzene (CB), dichloromethane, methanol, dimethyl sulfoxide (DMSO), and acetonitrile) and (d) the presence of different Lewis acids (see panel (f)). (e) and (f) Absorption maxima of the longer-wavelength band from the spectra in (c) and (d), respectively, plotted as a function of solvent/Lewis acid (see also Fig. S1 and S2).

of near-infrared absorption, positions these scaffolds as powerful candidates for high-contrast optical sensing. Realizing this potential, however, requires decoupling the intrinsic environmental sensitivity of the chromophore's electronic structure from perturbations introduced by the activating stimulus.

To address this need, we present a comprehensive investigation of the steady- and excited-state photophysical properties of a tetraarylallene in the presence of two distinct activating stimuli: solvent polarity and acid coordination. Systematic variation of solvent polarity reveals pronounced solvatochromism in the delocalized allylic cation, highlighting the strong sensitivity of its photophysical response to the surrounding medium. Consistent with these steady-state spectral shifts, the excited-state dynamics are likewise solvent-dependent, with less polar solvents stabilizing the ICT state and thereby prolonging the excited-state lifetime. We further demonstrate that aprotic Lewis acids can induce a coordinated state analogous to the allylic cation. In contrast to the pronounced sensitivity to the solvent environment, the identity of the acid has no measurable effect on the photophysical properties, thereby significantly expanding the range of chemical stimuli available for optical modulation. Ground-state density functional theory (DFT) calculations of the protonated species confirm the extended electronic delocalization of the intrinsic cation, while time-dependent DFT (TD-DFT) closely reproduces the experimentally observed solvent-dependent spectral features. Together, these findings reveal a key contrast: solvent polarity strongly modulates CT character and photophysics, whereas acid coordination produces an analogous state that is largely independent of acid identity. This distinction establishes design principles for broadly addressable, environmentally responsive optical materials.

Results and discussion

The chemical structure of the allene investigated in this work is shown in Fig. 1a. This compound features strongly electron-donating groups (NMe_2 and NPh_2) at one terminus of the allene and a strongly electron-withdrawing moiety (2,4,6-triphenyl-1,3,5-triazine) at the opposite terminus, forming an intramolecular donor–acceptor pair. In our previous work, we demonstrated that this configuration induces a pronounced bathochromic shift between the absorption maxima of the neutral allene and the allylic cation formed upon protonation.[11] Building on these initial findings, we investigated how additional activating stimuli and solvent environments modulate the photophysical response of this system. Understanding this interplay is critical for decoupling the intrinsic environmental sensitivity of the chromophore from perturbations introduced by the activating trigger, a key requirement for the design of robust, stimuli-responsive optical materials.

Fig. 1c shows the normalized steady-state absorption spectra of the allene after protonation with the Brønsted acid trifluoroacetic acid in a range of solvents of varying polarity. Two prominent absorption bands are observed at ~550 nm and ~700 nm, arising from the extended π-conjugation network of the molecule (Fig. 1b). While the molecule contains five chemically distinct Lewis basic sites, previous computational screening of all plausible protonation sites, including doubly protonated species, confirmed that only coordination at the central sp-hybridized carbon leads to the observed absorption features; protonation at peripheral sites alone does not produce the redshifted absorption.[11] To elucidate the origins of the observed dual-band absorption profile, we computed the vertical electronic transitions of the protonated allene using

TD-DFT (ωB97X-D3/def2-TZVP). The results reveal two primary low-energy transitions that reproduce the experimental spectral shape (Fig. S3). The lowest-energy transition (S_1) occurs at 2.41 eV and is dominated by a HOMO → LUMO excitation (87%). A second optically active transition (S_2) is predicted at 2.65 eV, originating predominantly from a HOMO−1 → LUMO excitation (82%). Although systematic screening of functionals, basis sets, and optimization protocols did not significantly improve the absolute energies (Fig. S4 and S5), the calculated vertical excitation energies show a consistent blueshift of ∼0.6 eV relative to experiment. This deviation is not unexpected, as range-separated hybrid functionals are known to overestimate excitation energies, particularly in extended π systems.[41–44] Nevertheless, the calculated energy gap between the S_1 and S_2 states accurately reproduces the relative spacing of the two visible/near-infrared absorption bands characteristic of the extended polymethine-like cation.

As shown in Fig. 1e and Fig. S1 and S2, both absorption bands exhibit pronounced solvatochromism, undergoing an overall redshift as the solvent is varied from polar acetonitrile to less polar solvents such as chlorobenzene (CB), and further into the nonpolar regime (hexane). Chlorinated solvents deviate from this trend, likely due to their higher polarizability, which leads to stronger interactions with the cationic solute. The observed negative solvatochromism indicates significant ICT character in these transitions, with a more polar cationic ground state than the excited state, such that nonpolar solvents destabilize the ground state and reduce the energy gap, whereas polar solvents stabilize the ground state and increase the energy gap.[45,46]

To determine whether the photophysical response can be modulated independently of the activating stimulus, we explored aprotic Lewis acids as alternative chemical activators (Fig. 1d). While traditional pH-responsive systems are constrained by the pK_a, a parameter defined by proton activity, Lewis acid activation is not governed by an equivalent thermodynamic descriptor; accordingly, the neutral allene in dichloromethane was titrated with a series of Lewis acids. We first examined the effect of counterion using a series of highly acidic boron salts (BF_3, BCl_3, BBr_3, and $B(C_6F_5)_3$). We then compared the influence of the Lewis acidic center by substituting boron with zinc and tin analogues ($ZnCl_2$, $ZnBr_2$, and $SnCl_2$).[47,48]

Similar to the spectra of the trifluoroacetic acid-protonated species, treatment with Lewis acids produces the same dual absorption features at ∼550 nm and ∼700 nm (Fig. 1d). Crucially, the identity of the Lewis acid has no measurable effect on the peak positions (Fig. 1f and Fig. S1), suggesting that no tight ion pairing occurs between the acid and the allylic cation.[49] In other words, the electrophile acts as a purely structural "switch," abstracting electron density to trigger π-electron reorganization without further perturbing the electronic landscape through coordination effects. This behavior indicates that the photophysical properties are intrinsic to the delocalized allylic cation rather than the specific acid–base adduct, establishing these allenes as robust platforms for multi-stimuli-responsive materials with a trigger-independent optical readout.

This interpretation is reinforced by ground-state DFT calculations (ωB97X-D3/def2-TZVP) performed using the ORCA 6.0.1 package,[50] where geometry optimizations of both the protonated and Lewis acid-coordinated allene (BF_3-coordinated) reveal delocalization of the molecular orbitals across the allylic bridge, forming an extended π system (Fig. S6). Comparison of the bond-length alternation (BLA) values obtained from DFT calculations suggests a very similar electronic character for both activation modes, with average path BLA values of 0.054 Å for the protonated species and 0.053 Å for the BF_3-coordinated complex (Fig. 2). These small and nearly identical BLA values further support that the electronic structure is primarily an intrinsic property of the delocalized allylic cation, effectively decoupled from the specific activating stimulus. Together, these experimental and computational results point to a unified conclusion: ground-state delocalization in the allylic cation is largely independent of the identity of the activating acid, consistent with early NMR studies demonstrating intrinsic charge delocalization in stable allylic frameworks.[49] This finding has important implications for materials design, demonstrating that activation can be decoupled from counterion effects, thereby enabling the use of a broad range of chemical stimuli without significantly perturbing the intrinsic optical response of the material.

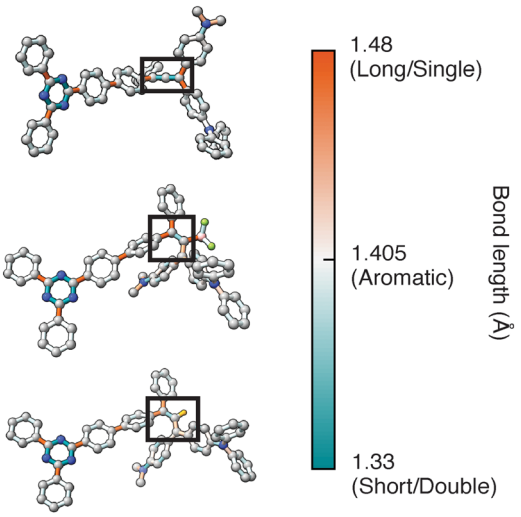

Fig. 2 Optimized molecular geometries of the neutral allene (top) and its corresponding BF_3 (middle) and H^+ (bottom) adducts. The structures are color-coded to represent calculated bond lengths, ranging from 1.33 Å (short/double bonds, teal) to 1.48 Å (long/single bonds, orange). The black boxes highlight the central structural motifs that undergo significant changes in bond length upon complexation or protonation. All hydrogen atoms, except for the protonating H^+ (shown in yellow), are omitted for clarity.

Femtosecond transient absorption (TA) experiments were performed to characterize the excited-state photophysical properties of the activated allene. The neutral allene, which serves as the unactivated precursor, absorbs predominantly in the ultraviolet region,[11] outside the spectral window accessible with our pump–probe setup. Accordingly, the present TA analysis focuses on the activated species, which share a common visible/near-infrared absorption and can be directly compared under identical conditions. TA maps of the trifluoroacetic acid–protonated allene in different solvents over the first 25 ps are shown in Fig. 3a–f. The

spectral profiles are largely similar across all solvents, exhibiting two negative features near 550 and 700 nm arising from ground-state bleach (GSB) of the protonated allene, consistent with the dual-peak structure observed in the steady-state absorption spectra. Notably, the positions of these features exhibit solvent-dependent shifts that mirror those observed in the steady-state solvatochromism. In dichloromethane and CB, the solvents that exhibit the largest redshifts of the peaks, an additional positive feature appears on the blue side of the GSB, arising from excited-state absorption (ESA) to higher-lying states. This feature is not observed in the other solvents, most likely because it lies outside the spectral detection window.

Despite the similarity in the spectral profiles, the decay dynamics exhibit pronounced solvent dependence (Fig. 3g, h and Tables S1 and S2). The decay traces are best described by one or two exponential components; traces in weakly polar solvents (toluene, chloroform, and CB) are best fit by a biexponential model, whereas those in dichloromethane, methanol, and acetonitrile are well described by a single component. This difference suggests that in weakly polar solvents, the excited-state population evolves through at least two distinct pathways, likely reflecting contributions from both locally excited and partially CT states arising from incomplete solvent stabilization. In contrast, in more polar solvents, rapid solvation stabilizes a single dominant excited-state configuration, leading to effectively single-exponential relaxation dynamics. For comparison of the overall decay kinetics, we report the amplitude-weighted average lifetime (τ_{avg}) for each solvent in Fig. 3h, which reduces to the single-component lifetime for monoexponential decays. τ_{avg} shows a clear and gradual decrease with increasing solvent polarity, from approximately 17.5 ps in the least polar solvent (toluene) to 2.0 ps in the most polar solvent (acetonitrile), indicating that increased solvent polarity stabilizes a more strongly charge-separated excited state with enhanced nonradiative decay. Ultrafast excited-state decay on few-picosecond timescales is commonly observed in conjugated systems and can arise from a range of nonradiative pathways. While conical intersections have been implicated in systems such as stilbene derivatives,[51,52] the pronounced solvent dependence and lack of viscosity dependence observed here (Fig. S7 and Table S3) suggest that the relaxation is primarily governed by the intrinsic ICT character of the delocalized allylic cation, rather than by structural dynamics. Overall, these results highlight the exceptional sensitivity of the allylic cation, with its excited-state lifetime varying by an order of magnitude with solvent polarity, underscoring its promise for future stimuli-responsive optical materials.

Fig. 4a–e shows the TA spectra measured on the allene dissolved in dichloromethane and activated by five different Lewis acids—BCl_3, BBr_3, $ZnCl_2$, $ZnBr_2$, and $SnCl_2$. Measurements could not be performed with BF_3 or $B(C_6F_5)_3$, as both acids reacted with the quartz cuvette. The TA maps exhibit two negative features near 550 and 700 nm arising from GSB, in good agreement with the steady-state absorption profiles, and a positive ESA feature also appears on the blue edge of the spectra. In contrast to the solvent-dependent case, no measurable shift in peak position is observed as a function of the Lewis acid identity; the positions of both GSB bands are consistent with those observed for the protonated allene in dichloromethane (Fig. 3d), again indicating that the photophysical response is determined by the intrinsic electronic structure of the allylic cation and is insensitive to the identity of the Lewis acid. Consistent with the spectral features, the decay profiles are identical across all Lewis acids and are well described by a monoexponential model, with a time constant of approximately

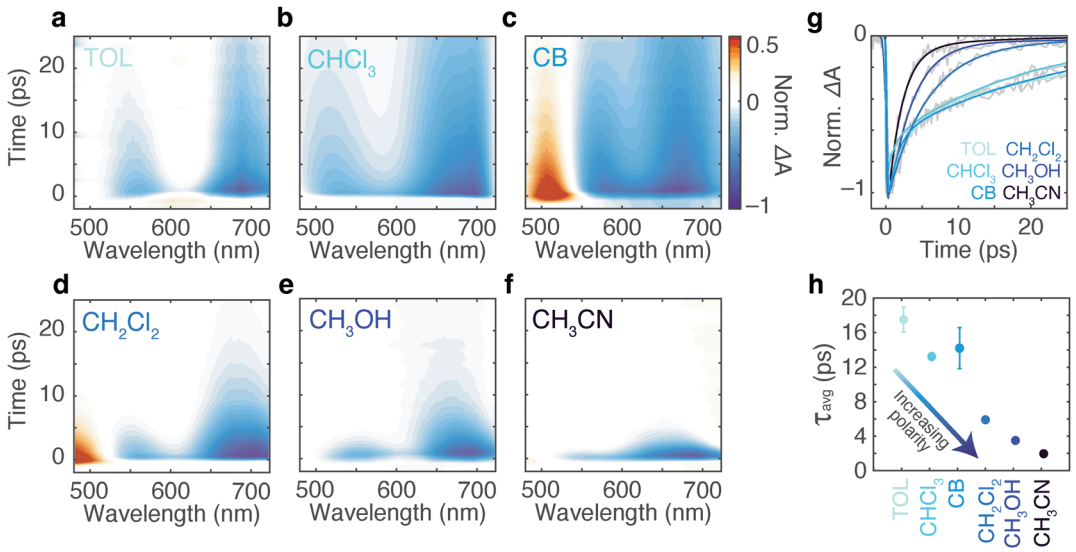

Fig. 3 (a)–(f) TA spectra of the allene protonated with trifluoroacetic acid in (a) toluene (TOL), (b) chloroform, (c) chlorobenzene (CB), (d) dichloromethane, (e) methanol, and (f) acetonitrile, over the initial 25 ps. (g) Normalized exponential fits to the kinetic traces, extracted at the maximum of the most intense GSB feature: 687 (toluene), 690 (chloroform), 670 (chlorobenzene), 687 (dichloromethane), 687 (methanol), and 684 nm (acetonitrile). (h) Weighted average decay constants (τ_{avg}) obtained from the fits. Error bars indicate 95% confidence intervals of the fit. Full details of the fit parameters, including the individual time constants and corresponding amplitudes, are provided in Tables S1 and S2.

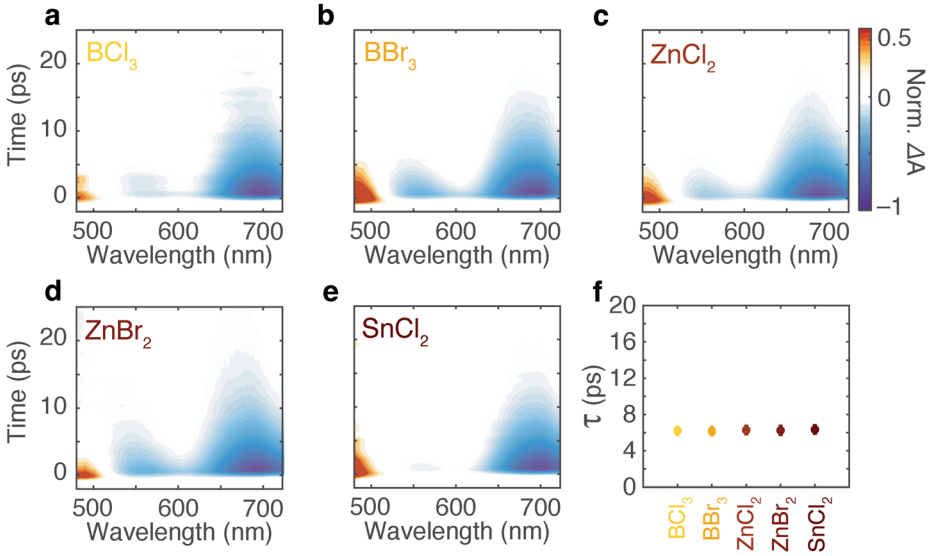

Fig. 4 (a)–(e) TA spectra of the allene activated with Lewis acids (a) BCl_3, (b) BBr_3, (c) $ZnCl_2$, (d) $ZnBr_2$, and (e) $SnCl_2$, shown over the initial 25 ps. (f) Decay constants (τ) obtained from monoexponential kinetic fits at the maximum of the most intense GSB feature for each Lewis acid: 690 (BCl_3), 683 (BBr_3), 694 ($ZnCl_2$), 689 ($ZnBr_2$), and 700 nm ($SnCl_2$). Error bars indicate 95% confidence intervals of the fit. Full details of the fit parameters, including the individual time constants, are provided in Tables S4 and S5.

6 ps (Fig. 4f and Tables S4 and S5). These results demonstrate that the excited-state kinetics of the activated allene are insensitive to the identity of the activating agent and instead are governed by the solvent environment, reinforcing the notion that activation serves primarily as a structural trigger while leaving the underlying photophysical landscape largely unchanged. This robustness highlights the potential of these systems as versatile platforms for stimuli-responsive optical materials with consistent and predictable photophysical behavior.

Conclusions

In conclusion, we have performed a detailed study of the photophysical properties of highly delocalized allylic cations generated from a donor–acceptor substituted allene. We have demonstrated that the optoelectronic properties are fundamentally governed by the local solvent environment rather than the specific identity of the activating chemical stimulus. Activation *via* either the Brønsted acid trifluoroacetic acid or a variety of Lewis acids generates an extended polymethine-like CT state with identical spectral signatures in the steady state and excited state. Both steady-state and femtosecond TA measurements reveal pronounced negative solvatochromism, demonstrating that less polar solvents stabilize the ICT state and significantly prolong excited-state lifetimes. In contrast, the electronic structure and optical transitions are intrinsic to the delocalized allylic cation network and are effectively independent of counterion identity and specific ion-pairing interactions. Ultimately, the ability to reversibly trigger these strongly absorbing, near-infrared states using a diverse array of electrophiles, without altering the optical readout, establishes this tetraarylallene scaffold as a versatile and robust platform for the design of next-generation stimuli-responsive optical materials and environmental sensors.

Methods

Sample preparation

Activation of the allene was achieved through the addition of trifluoroacetic acid or a Lewis acid (BF_3, BCl_3, BBr_3, $B(C_6F_5)_3$, $ZnCl_2$, $ZnBr_2$, and $SnCl_2$) to a solution of the neutral compound. All Lewis acid measurements were conducted in dichloromethane. All solvents and Lewis acids were purchased as ACS-grade reagents from commercial suppliers and used as received without further purification.

General electronic structure calculations

All DFT and TD-DFT calculations were performed using the ORCA quantum chemistry package (version 6.0.1). Ground-state geometries were optimized with both B3LYP and ωB97X-D3 to assess the influence of the starting structure on the predicted photophysical properties. Vertical excitation energies were then computed using TD-DFT with ωB97X-D3, CAM-B3LYP, and M06-2X (see the SI for further details and additional computational data). The def2-TZVP basis set was employed for all atoms in both geometry optimizations and single-point calculations to ensure a consistent and high-quality description of the electronic structure. TD-DFT calculations were performed using the conductor-like polarizable continuum model (CPCM) with parameters for dichloromethane. The ten lowest singlet excited states (N_{roots} = 10) were computed using the Davidson algorithm, with convergence tolerances for the energy (ETol) and residual (RTol) set to 10^{-6}.

Steady-state absorption and emission spectroscopy

Steady-state absorption spectra were measured with a Cary 5000 UV-Vis-NIR spectrophotometer (Agilent) in a 2 mm quartz cuvette.

Ultrafast TA spectroscopy

Broadband TA measurements were performed using a home-built TA spectrometer. 1030 nm, 230 fs pulses were generated by a femtosecond Yb:KGW laser operating at a repetition rate of 100 kHz (PHAROS, Light Conversion). The 1030 nm fundamental was converted to 800 nm using an optical parametric amplifier (I-OPA-FW, Light Conversion) and compressed to a 40 fs pulse duration. The compressed 800 nm beam was subsequently split into pump and probe beams. The broadband light source for both the pump and the probe beams was produced using white-light generation by focusing the fundamental onto a 4-mm thick sapphire crystal. The white light for the pump and probe arms was generated separately. After collimation, the white light was filtered through a 750-nm short-pass filter to remove the intense residual 800 nm light (FESH0750, Thorlabs), and each arm was compressed separately using a pair of chirped mirrors (DCM9, Laser Quantum). A second-harmonic-generation frequency-resolved optical gating (SHG-FROG) measured a 20 fs duration for the compressed pulse for both arms (Fig. S8). The pump beam was modulated using an optical chopper (New Focus 3502) at 20 kHz. The pump–probe time delay was varied by delaying the probe pulse using a motorized translation stage (PRO115SL, Aerotech). Both beams were focused onto solution-phase samples contained in a quartz cuvette with a 500 μm pathlength. The pulse energy at the sample position was 0.167 μJ pulse^{-1} for the pump and 0.16 μJ pulse^{-1} for the probe. After the sample position, the pump beam was blocked, and the transmitted probe beam was routed toward a home-built spectrograph. The spectrally dispersed signal was detected at 100 kHz on a line CCD (Octoplus, Teledyne e2v).

Author contributions

J. Z. and M. J. synthesized the allene and performed steady-state spectroscopy. B. A. T., S. P., and R. M. G. performed the time-resolved spectroscopy experiments. N. W. and E. L. conducted steady-state Lewis acid studies. C. S. and M. S. conceived of the idea, co-wrote the manuscript, and supervised the project. All authors contributed to editing the manuscript.

Conflicts of interest

There are no conflicts to declare.

Data availability

The supporting data has been provided as part of the supplementary information (SI). Supplementary information: tables of fit parameters, supplementary experimental spectra and computational results. See DOI: https://doi.org/10.1039/d6ma00475j.

Acknowledgements

The work at Boston University was supported by startup funds. B. A. T., S. P., R. M. G. and M. S. acknowledge the use of the Boston University Photonics Center shared facilities. R. M. G. acknowledges support from National Science Foundation Training Grant No. DGE-2244216. C. S. gratefully acknowledges financial support from the National Science Foundation through the CAREER program (Grant No. 2541093).

References

1 X. Chen, M. A. Dam, K. Ono, A. Mal, H. Shen, S. R. Nutt, K. Sheran and F. Wudl, *Science*, 2002, **295**, 1698–1702.
2 K. T. Oh, H. Yin, E. S. Lee and Y. H. Bae, *J. Mater. Chem.*, 2007, **17**, 3987–4001.
3 B. Ghosh and M. W. Urban, *Science*, 2009, **323**, 1458–1460.
4 O. M. Wani, H. Zeng and A. Priimagi, *Nat. Commun.*, 2017, **8**, 15546.
5 S. J. Bailey, E. Hopkins, K. D. Rael, A. Hashmi, J. M. Urueña, M. Z. Wilson and J. Read de Alaniz, *Angew. Chem., Int. Ed.*, 2023, **62**, e202301157.
6 S. J. O'Neill, Y. C. Tse, Z. Huang, X. Chen, J. A. McCune and O. A. Scherman, *J. Am. Chem. Soc.*, 2025, **147**, 33337–33342.
7 S. Dolui, B. Sahu and S. Banerjee, *Macromol. Chem. Phys.*, 2025, **226**, 2400472.
8 P. Theato, B. S. Sumerlin, R. K. O'Reilly and T. H. Epps III, *Chem. Soc. Rev.*, 2013, **42**, 7055–7056.
9 Z. Zhang, A. Mei, W. Wang, K. Xu, M. Wang, P. Chen, J. Shao and X. Dong, *Coord. Chem. Rev.*, 2025, **545**, 217026.
10 Z. Zhang, Q. Bai, Z. Zhai, Q. Long, E. Han, H. Zhao, C.-W. Zhou, H. Lin, W. Zhang and G.-H. Ning, *et al.*, *Nat. Commun.*, 2024, **15**, 7261.
11 J. Zhao, L. Jiao, L. Kinziabulatova, T. J. Williams, R. M. Gracia, A. Gartner, T. A. Stich, W. Ding, M. Son and C. Schaack, *J. Am. Chem. Soc.*, 2025, **147**, 32710–32716.
12 P. Kulkarni, M. K. Haldar, S. You, Y. Choi and S. Mallik, *Biomacromolecules*, 2016, **17**, 2507–2513.
13 K. Ansorg, H. Braunschweig, C.-W. Chiu, B. Engels, D. Gamon, M. Hügel, T. Kupfer and K. Radacki, *Angew. Chem., Int. Ed.*, 2011, **50**, 2833.
14 R. Haag and F. Kratz, *Angew. Chem., Int. Ed.*, 2006, **45**, 1198–1215.
15 Z. Zhao, H. Meng, N. Wang, M. J. Donovan, T. Fu, M. You, Z. Chen, X. Zhang and W. Tan, *Angew. Chem., Int. Ed.*, 2013, **125**, 7487–7491.
16 L. Li, J. Yin, W. Ma, L. Tang, J. Zou, L. Yang, T. Du, Y. Zhao, L. Wang and Z. Yang, *et al.*, *Nat. Mater.*, 2024, **23**, 993–1001.
17 P. Athira, R. N. Kappumchalil, A. R. Sachin, M. Yoosuf, R. Thomas and G. Gopakumar, *J. Phys. Chem. A*, 2024, **128**, 3935–3946.
18 Y. I. Park, O. Postupna, A. Zhugayevych, H. Shin, Y.-S. Park, B. Kim, H.-J. Yen, P. Cheruku, J. Martinez and J. Park, *et al.*, *Chem. Sci.*, 2015, **6**, 789–797.
19 Y. Bo, Y. Hou, D. A. Lavergne, T. Clark, M. J. Ferguson, R. R. Tykwinski and D. M. Guldi, *Nat. Commun.*, 2025, **16**, 2968.
20 A. S. Klymchenko, *Acc. Chem. Res.*, 2017, **50**, 366–375.
21 P. Chowdhury, B. Saha, K. Bauri, B. S. Sumerlin and P. De, *J. Am. Chem. Soc.*, 2024, **146**, 21664–21676.
22 N. Mataga, Y. Kaifu and M. Koizumi, *Bull. Chem. Soc. Jpn.*, 1956, **29**, 465–470.

23 A. Painelli and F. Terenziani, *J. Phys. Chem. A*, 2000, **104**, 11041–11048.
24 V. S. Pavlovich, *ChemPhysChem*, 2012, **13**, 4081–4093.
25 W. Kanezaki, R. Ishikawa and H. Tsuji, *Eur. J. Org. Chem.*, 2025, e202401471.
26 F. Bureš, *RSC Adv.*, 2014, **4**, 58826–58851.
27 Y. Li, M. Zhou, Y. Niu, Q. Guo and A. Xia, *J. Chem. Phys.*, 2015, **143**, 034309.
28 P. K. Samanta and R. Misra, *J. Appl. Phys.*, 2023, **133**, 020901.
29 S. Debnath, A. Mohanty, P. Naik, U. Salzner, J. Dasgupta and S. Patil, *J. Mater. Chem. C*, 2024, **12**, 9200–9209.
30 C. T. Martins, M. S. Lima and O. A. El Seoud, *J. Org. Chem.*, 2006, **71**, 9068–9079.
31 C. T. Martins, M. S. Lima, E. L. Bastos and O. A. El Seoud, *Eur. J. Org. Chem.*, 2008, 1165–1180.
32 E. Buncel and S. Rajagopal, *Acc. Chem. Res.*, 1990, **23**, 226–231.
33 Ó. Guzmán-Méndez, M. M. Reza, B. Meza, J. Jara-Cortés and J. Peón, *J. Phys. Chem. B*, 2023, **127**, 5655–5667.
34 G. S. Loving, M. Sainlos and B. Imperiali, *Trends Biotechnol.*, 2010, **28**, 73–83.
35 M. C. Rezende, *J. Phys. Org. Chem.*, 2016, **29**, 460–467.
36 A. V. Kulinich, E. K. Mikitenko and A. A. Ishchenko, *Phys. Chem. Chem. Phys.*, 2016, **18**, 3444–3453.
37 E. V. Verbitskiy, E. M. Dinastiya, A. A. Baranova, K. O. Khokhlov, R. D. Chuvashov, Y. A. Yakovleva, N. I. Makarova, E. V. Vetrova, A. V. Metelitsa and P. A. Slepukhin, *et al.*, *Dyes Pigm.*, 2018, **159**, 35–44.
38 J. H. van't Hoff, *The Arrangement of Atoms in Space*, Longmans, Green and Company, 1898.
39 P. Maitland and W. Mills, *Nature*, 1935, **135**, 994.
40 A. Pareek, Y. Qiu, M. A. Johnson, R. R. Tykwinski and P. Gaweł, *Chem. Sci.*, 2026, **17**, 791–830.
41 Y.-S. Lin, G.-D. Li, S.-P. Mao and J.-D. Chai, *J. Chem. Theory Comput.*, 2013, **9**, 263–272.
42 J. C. Garcia-Alvarez and S. Gozem, *J. Chem. Theory Comput.*, 2024, **20**, 7227–7243.
43 D. Jacquemin, V. Wathelet, E. A. Perpète and C. Adamo, *J. Chem. Theory Comput.*, 2009, **5**, 2420–2435.
44 A. D. Laurent and D. Jacquemin, *Int. J. Quantum Chem.*, 2013, **113**, 2019–2039.
45 T. L. Cecil and S. C. Rutan, *Anal. Chem.*, 1990, **62**, 1998–2004.
46 S. Spange and T. G. Mayerhöfer, *ChemPhysChem*, 2022, **23**, e202200100.
47 A. E. Laturski, J. R. Gaffen, P. Demay-Drouhard, C. B. Caputo and T. Baumgartner, *Precis. Chem.*, 2023, **1**, 49–56.
48 J. R. Gaffen, J. N. Bentley, L. C. Torres, C. Chu, T. Baumgartner and C. B. Caputo, *Chemistry*, 2019, **5**, 1567–1583.
49 G. A. Olah, P. R. Clifford, Y. Halpern and R. G. Johanson, *J. Am. Chem. Soc.*, 1971, **93**, 4219–4222.
50 F. Neese, *Wiley Interdiscip. Rev.: Comput. Mol. Sci.*, 2025, **15**, e70019.
51 S. Takeuchi, S. Ruhman, T. Tsuneda, M. Chiba, T. Taketsugu and T. Tahara, *Science*, 2008, **322**, 1073–1077.
52 Otolski, A. Mohan Raj, G. Sharma, R. Prabhakar, V. Ramamurthy and C. G. Elles, *J. Phys. Chem. A*, 2019, **123**, 5061–5071.